Stress corrosion behaviour of high-strength steel: the role of fatigue

pre-cracking

J. Toribio and V. Kharin#

Department of Materials Science, University of La Coruña

ETSI Caminos, Campus de Elviña, 15071 La Coruna, Spain Tel: (34-981) 16 70 00; Fax: (34-981) 16 71 70

*on leave from: Pidstryhach Institute for Applied Mechanics and Mathematics, Lviv, Ukraine

Abstract

This paper analyzes the role of fatigue pre-cracking in the stress corrosion behaviour of high strength

pearlitic steel subjected to localised anodic dissolution and hydrogen assisted cracking. The effects of

crack-tip plastic straining and crack-tip residual stresses of a compressive nature, generated by fatigue

loading, are elucidated by using both a simple theoretical estimation and a high-resolution numerical

modelling of the near-tip stress-strain field during the previous cyclic loading and the posterior

monotonic loading. It is shown that cyclic crack tip plasticity improves the stress corrosion behaviour of

the steel in the two regimes of cracking. In the respective cases, the effects are supposed to be due to

accelerated local anodic dissolution of the cyclic plastic zone (cumulative damage region) producing

chemical crack blunting or to the delay of hydrogen entry into the metal caused by compressive

residual stresses, thus increasing in both cases the fracture load in aggressive environment.

Keywords: stress corrosion cracking, crack-tip residual stresses, cyclic plastic zone.

1. INTRODUCTION

Stress corrosion cracking (SCC) of metals and alloys is evaluated in laboratory testing of

pre-cracked specimens /1/. Thus, a pre-crack in the specimen is required, and it is usually

generated by fatigue (cyclic) loading in air environment. Fatigue pre-cracking inevitably

produces a substantial redistribution of stresses and strains in the near-tip zone, which may

affect the posterior stress corrosion behaviour /2/.

205

The influence of pre-loading on SCC has been studied in several works /2-4/. Pre-cracking at higher values of the stress intensity factor range $\Delta K = K_{max} - K_{min}$, where K_{max} and K_{min} are respectively the maximum and minimum values of the stress intensity factor K during fatigue, produces a retarding effect on SCC. This is explained usually by the action of compressive residual stresses produced near the crack tip at load reversals due to accumulated plastic deformation.

This paper offers an analysis —both theoretical and numerical— of the mechanical aspects of the effect of the fatigue pre-cracking regime on the posterior SCC in a high-strength steel. To this end, the rising load SCC experiments are considered in combination with a simple theoretical estimation and a high-resolution numerical modelling of the elastoplastic stress-strain field in the vicinity of the crack tip subjected to fatigue pre-cracking and subsequent monotonic loading up to the points of fracture in SCC tests.

2. EXPERIMENTAL

The aim of this paper is to analyze the consequences of fatigue pre-cracking on the posterior stress corrosion behaviour of the high-strength steel. Different zero-to-tension cyclic loading levels were used in the experiments, the key variable being the maximum stress intensity factor at the last stage of the pre-cracking K_{max} , whereas $K_{min} \approx 0$ in all tests. Four different fatigue programmes were performed with $K_{max}/K_{IC}=0.28$, 0.45, 0.60 and 0.80, where K_{IC} is the fracture toughness in the absence of harsh environment.

A high-strength steel was studied whose chemical composition and mechanical properties are given respectively in Tables 1 and 2. The SCC experiments were slow strain rate tests /5/ with pre-cracked specimens in aqueous solution, as described in detail elsewhere /2/. The tests were performed at anodic and cathodic potentials to evaluate the two main mechanisms of SCC: localised anodic dissolution (LAD) and hydrogen assisted cracking (HAC). Fig. 1 shows the

Table 1 Chemical composition (wt %) of the steel

С	Mn	Si	P	S	Cr	Ni	Мо
0.74	0.70	0.20	0.016	0.023	0.01	0.01	0.001

Table 2 Mechanical properties of the steel

Young mod. Yield Stress E σ_Y		$UTS \\ \sigma_R$	Toughness K _{IC}	Ramberg-G Section I (El	_	$\varepsilon = \varepsilon^{e} + \varepsilon^{p} = \sigma/E + (\sigma/P)^{n}$ Section II ($\varepsilon^{p} > 1.07$)	
(GPa)	(MPa)	(MPa)	(MPam ^{1/2})	P _I (MPa)	n_{I}	P _{II} (MPa)	nII
195	725	1300	53	2120	5.8	2160	17

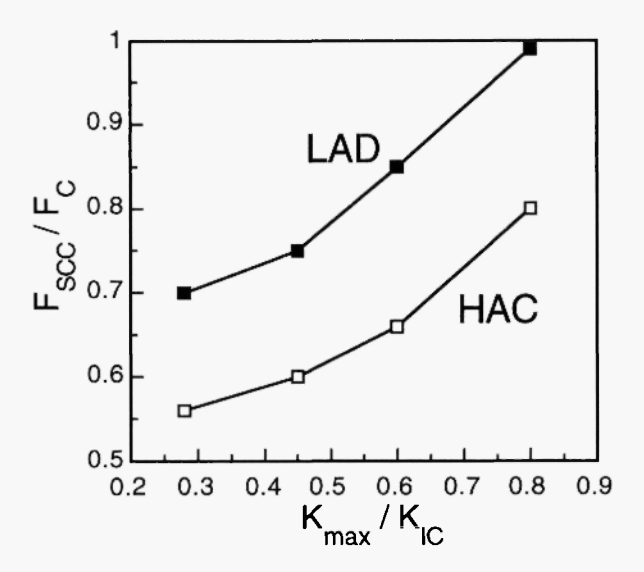


Fig. 1: SCC test results in terms of respective fracture loads in aggressive and inert (laboratory air) environments at the anodic regime (-400 mV vs. SCE: LAD) and at the cathodic regime (-1200 mV vs. SCE: HAC).

experimental results of the failure load in solution F_{SCC} (divided by the reference value at rupture in air F_C) as a function of the ratio K_{max}/K_{IC} . For both regimes of cracking, the

mechanical effect of fatigue pre-cracking is beneficial for the SCC resistance of the steel, since the fracture load in aggressive environment is an increasing function of K_{max} .

These phenomena may be caused by the development of the cyclic plastic zone and the presence of compressive stresses (cyclic residual stresses) in the vicinity of the crack tip as a consequence of the fatigue pre-cracking procedure. The crack tip is pre-strained (and in a certain sense pre-stressed) by fatigue: the higher the cyclic load level, the more pronounced is the pre-straining/stressing effect which delays the environmental damage process (metal dissolution or hydrogen entry in respective cases of LAD and HAC) and improves material performance.

To ascertain the mechanical effects of the pre-cracking regime on SCC, it is desired to know the evolution of certain mechanical variables associated with the environmentally assisted cracking processes. The items of primary interest are the variations of the plastic zone (Fig. 2) and the stress distribution beyond the crack tip affected by cyclic pre-loading. In particular, hydrostatic stress σ plays a fundamental role in HAC processes driven by stress-assisted hydrogen diffusion /6/. To represent the theoretical and numerical results, the two usual coordinate systems —cartesian and polar— attached to the common origin at the crack tip were used, as shown in Fig. 2.

3. THEORETICAL MODELLING OF NEAR-TIP FIELDS

In the previous analyses /4,7/, the superposition approach by Rice /8/ was applied to elucidate these matters. Restricted by crucial simplistic assumptions, it captures roughly some trends but misses substantial features of the near tip elastoplastic stress-strain field evolution. The next section of this paper offers a high-resolution numerical modelling of these cyclic residual stresses in the vicinity of the crack tip after loading-unloading the specimen, and an improved calculation of the evolutions of plastic zone and stress-strain distributions in the

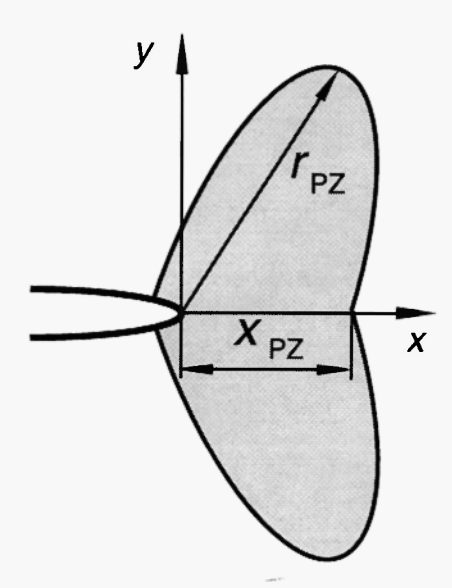


Fig. 2: Scheme of the coordinate systems attached to the crack tip and characteristic dimensions of the plastic zone.

vicinity of a crack tip subjected to rising load SCC tests. However, the simple Rice model may be used as a first approach to obtain a fast and easy theoretical estimation.

Fig. 3 offers a schematic representation of the monotonic (for $K=K_{max}$) and cyclic (for $K=K_{min}$) stress distribution ahead of a crack tip which has been subjected to cyclic zero-to-tension loading, according to the superposition considerations of the Rice model for an elastic ideally plastic material /8/. On adapting this model for the plane strain case by using an *effective* (constrained) yield stress σ_Y^* /8/ as modified by the stress triaxiality according to the Irwin estimate of the near tip plasticity constraint factor (cf. /8,9/), it is possible to obtain the depths $x_{PZ}^{(R)}$ and $\Delta x_{PZ}^{(R)}$ of, respectively, the *forward* (or *monotonic*, at K_{max}) and *reversed* (or *cyclic*, at K_{min}) plastic zones beyond the crack tip in a perfectly plastic solid (with *no strain hardening*) as follows:

$$x_{PZ}^{(R)}(K_{max}) = \frac{1}{3\pi} \left(\frac{K_{max}}{\sigma_Y}\right)^2$$
 (1)

$$\Delta x_{PZ}^{(R)}(\Delta K) = \frac{1}{3\pi} \left(\frac{\Delta K}{2\sigma_{Y}}\right)^{2} = \frac{1}{4} x_{PZ}^{(R)}(\Delta K)$$
 (2)

where σ_Y is the tensile yield stress, and the superindex (R) refers to the Rice estimation. In the tests presented in this work, $K_{min} \approx 0$, and therefore $\Delta K \approx K_{max}$. With the mentioned plane strain plasticity constraint factor after Irwin, the extreme normal stress in the crack plane σ_{yy} alternates between $\pm \sigma_Y^*$, i.e., its maximum absolute value is the effective (constrained) yield stress $\sigma_Y^* = \sqrt{3}\sigma_Y$ (cf. /9/), as shown in Fig. 3. The hydrostatic stress cycling proceeds between $\pm \sigma^*$, where $\sigma^* = 8/(3\sqrt{3})\sigma_Y \approx 1.54\sigma_Y$ (see Fig. 3). The plastic zone itself "pulsates" within the range from $\Delta x_{PZ}^{(R)}$ at K_{min} to $x_{PZ}^{(R)}$ at K_{max} . In addition, it is clear from Fig. 3 that $\Delta x_{PZ}^{(R)}$ represents the depth of maximum compression next to the crack tip at K_{min} , whereas $x_{PZ}^{(R)}$

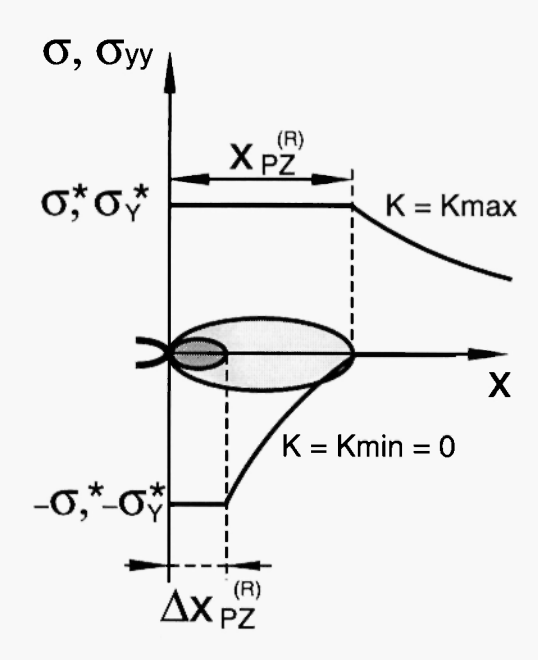


Fig. 3: Monotonic (for $K=K_{max}$) and cyclic (for $K=K_{min}=0$) stress distributions ahead of a crack tip which has been subjected to cyclic zero-to-tension loading, according to the Rice model for an elastic ideally plastic material /8/. The schema shows the distributions of both hydrostatic stress σ and uniaxial stress σ_{yy} (normal to the crack plane) and their maximum levels. The forward (or monotonic) plastic zone is lightly shadowed, whereas the reversed (or cyclic) plastic zone is densely shadowed.

gives the depth (measured from the crack tip) of the maximum hydrostatic stress point in both monotonic (K_{max}) and cyclic (K_{min}) loading.

4. NUMERICAL MODELLING OF NEAR-TIP FIELDS

4.1. Description of the numerical procedure

A more accurate approach to the problem of fatigue precracking by cyclic loading in real structural materials is performed by taking into account strain hardening effects in the material and modelling in detail the near-tip area in which the evolution of stress and strain is fundamental. In this section, the effect of fatigue pre-cracking is analyzed by high-resolution numerical modelling of the stress-strain state near the crack tip in a rate-independent elastoplastic material with von Mises yield surface and power-law strain hardening. A combined isotropic-to-kinematic hardening rule is used, which captures the effect of hysteresis loop stabilisation associated with cyclic stress-strain behaviour /10/. The mechanical characteristics of the material correspond to the steel used in the experimental programme (cf. Table 2).

Stress-strain fields in the close vicinity of the crack tip are known to depend substantially on the crack blunting /11,12/. To reveal them, finite deformation analysis of a plane strain crack subjected to mode I (opening) load was performed, confining the study to the small scale yielding situation, which allows a consideration of the stress intensity factor K as the only variable governing the near tip mechanical situation irrespective of a particular geometry of a cracked solid and applied load (cf. /9,11/). The crack was modelled as a parallel-sided round-tip slit with initial height (twice the tip radius) $b_0 = 5 \mu m$, which is in agreement with experimental data reported for fatigue cracks in steels /13/. The applied loading history consisted of several (up to ten) zero-to-tension cycles in accordance with most of the experimental fatigue programmes, namely, at $K_{max}/K_{IC} = 0.45$, 0.60 and 0.80, followed by rising load

corresponding to the SCC testing. The nonlinear finite element code MARC /14/ was used with updated Lagrangian formulation. The modelling peculiarities (solid's geometry, loading, etc.) are the same as described elsewhere /12/. In particular, after trying several refinements of the finite element mesh near the crack tip, the optimum one was chosen in which the average size of the smallest four-node quadrilateral elements adjacent to the tip was about 0.02b₀.

4.2. Stress-strain evolution

In contrast to the plastic zone analysis which should not be sensibly improved considering large geometry changes at the deformed crack tip, the near tip stress distributions must be very sensitive to the blunted tip geometry evolution /11,12/. Accordingly, the obtained near tip stress patterns differ substantially from the estimation proposed by Rice /8/.

As a general observation on cyclic stress distributions, for all load cases the bounds of alternation of the hydrostatic stress σ were more than $\pm 3.8\sigma_Y$, i.e., notably above the mentioned estimate of about $\pm 1.54\sigma_Y$ of the Rice model. This stress field component is focused since it is of major interest for HAC governed by stress-assisted hydrogen diffusion in metal /6/. Fig. 4 shows the evolution of the hydrostatic stress distribution in the plane of the crack beyond the tip, $\sigma = \sigma(x)$, where x is the distance in the *deformed* configuration of a solid, during monotonic loading in the SCC test after fatigue pre-cracking.

With regard to the depth of the points of minimum and maximum hydrostatic stress during fatigue pre-cracking with constant amplitude K_{max} , the specific depths always ranged as follows:

$$x_{\sigma(\min)} < x_{\sigma(\max)} \lesssim \frac{1}{3} \Delta x_{PZ}$$
 (3)

where $x_{\sigma(min)}$ and $x_{\sigma(max)}$ are respectively the depths of the historical minimum $\sigma_{(min)}$ (minimorum, for K_{min}) and historical maximum $\sigma_{(max)}$ (maximorum, for K_{max}) of hydrostatic stress, and Δx_{PZ} represents the depth of the cyclic plastic zone (i.e., for $K=K_{min}$) which is

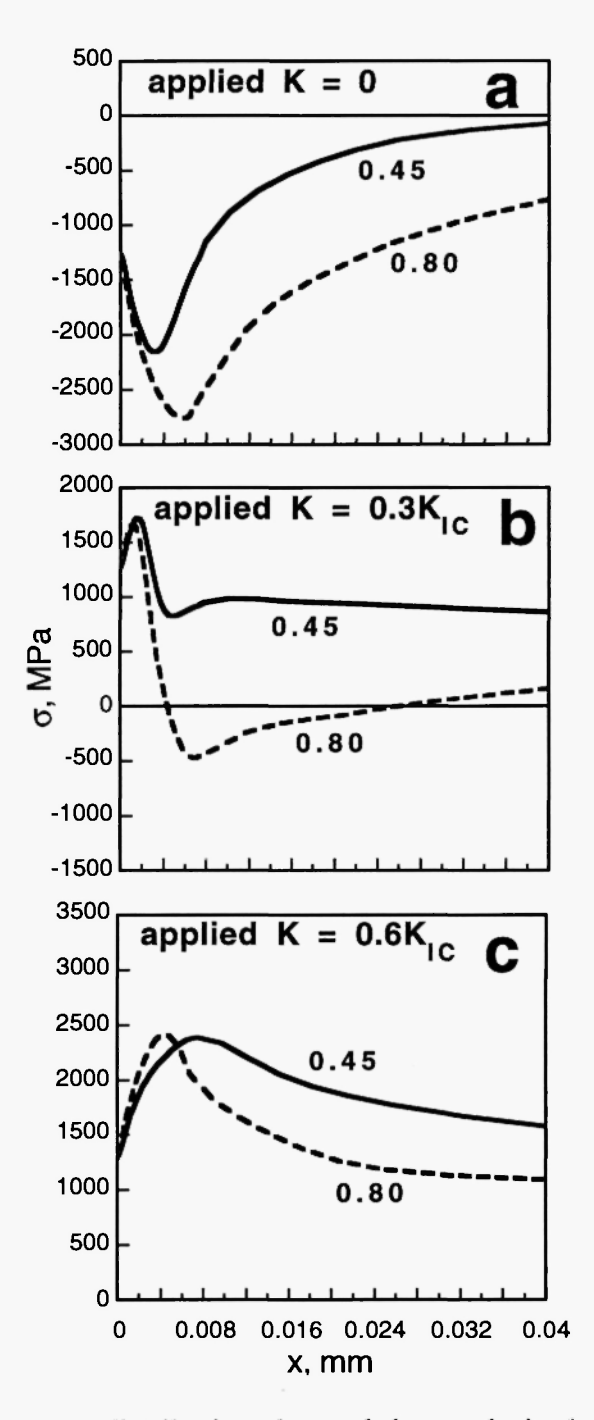


Fig. 4: Hydrostatic stress distributions beyond the crack tip during monotonic loading at SCC test after fatigue pre-cracking at $K_{max}/K_{IC} = 0.45$ (solid lines) and 0.8 (dashed lines) at progressive applied K levels indicated in the figures. The distance x from the crack tip is measured in the *deformed* configuration.

quite lower than the Rice estimation $\Delta x_{PZ}^{(R)}$. Thus, the maximum hydrostatic stress point is much closer to the tip than the prediction (1) of the Rice approach /8/.

As a consequence of the not perfectly plastic but work hardening material behaviour, the extrema of the hydrostatic stresses σ for the top and bottom of fatigue load cycles, $\sigma_{(min)}$ and $\sigma_{(max)}$, as well as their locations $x_{\sigma(min)}$ and $x_{\sigma(max)}$, depend on the applied load amplitude K_{max} and on the cycle number N: the absolute values of the σ -stress extrema increase slightly with a rise of either K_{max} or N, whereas their depths increase with K_{max} and decrease with N. However, these characteristics of the near tip stress-strain state should stabilise with the increase of N as soon as a steady state (stabilisation) of alternating plastic flow is approached, depending on the level of applied K_{max} .

With regard to the normal stress in the plane of the crack σ_{yy} , the patterns of $\sigma_{yy}(x)$ were quite similar to those displayed in Fig. 4, although the absolute values of the σ_{yy} -stress were greater, roughly by a factor of about 1.6. Comparing the distributions of the hydrostatic and normal stresses $\sigma(x)$ and $\sigma_{yy}(x)$ in each particular load case (i.e., fixed K_{max} -value during fatigue), their both extrema $\sigma_{(min,max)}$ and $\sigma_{yy(min,max)}$ were found at approximately the same depths $x = x_{\sigma(min,max)}$, at corresponding $K_{(min,max)}$ respectively.

4.3. Plastic zone development

Fig. 5 shows the plastic zones where the equivalent von Mises stress exceeds the tensile yield stress ($\sigma_{eq} > \sigma_Y$) at load maxima ($K = K_{max}$) and minima ($K = K_{min} = 0$) according to the numerical solutions. These zones are nearly invariable as the number of load cycles increases and their shapes appear approximately self-similar with a scaling factor of $(K_{max}/\sigma_Y)^2$, cf. Fig. 5. The performed finite element analysis provides the following estimation of the depth of the forward (monotonic) plastic zone at K_{max} :

$$x_{PZ}(K_{max}) = 0.034 \left(\frac{K_{max}}{\sigma_Y}\right)^2$$
 (4)

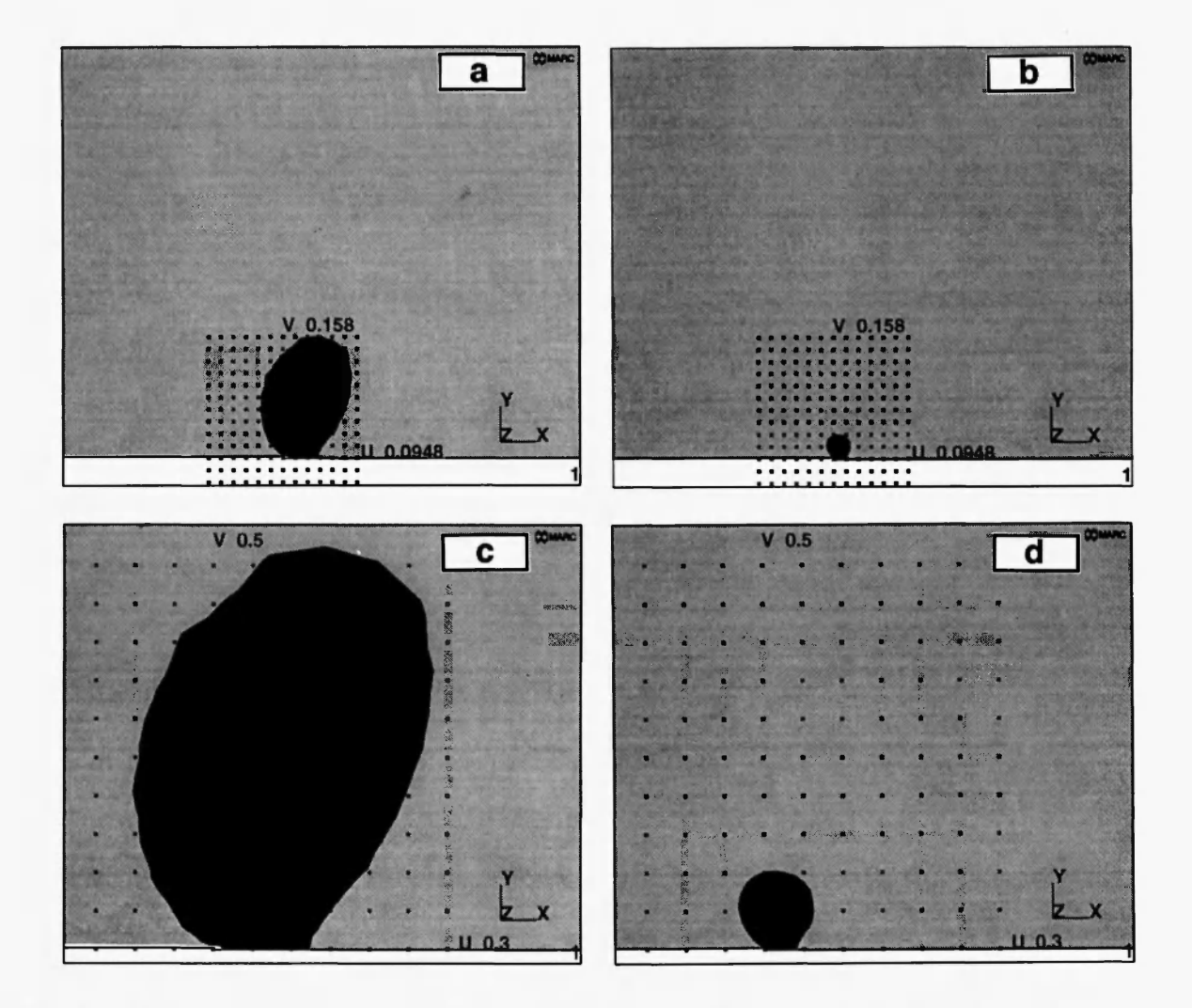


Fig. 5: Plastic zones $\sigma_{eq} \ge \sigma_Y$ under cyclic loading at $K_{max}/K_{IC} = 0.45$ (top pictures) and 0.8 (bottom pictures): (a/c) monotonic plastic zones at K_{max} ; (b/d) cyclic plastic zones at K_{min} ; all figures are in the same scale whereas the grids are scaled with the factor $(K_{max}/\sigma_Y)^2$ so the grid spacings are 0.016 mm in (a/b) and 0.050 mm in (c/d).

The reversed (cyclic) plastic zone at $K_{min} \approx 0$ is also dependent on the previous K_{max} -level (or, in other words, on the range ΔK). For strain hardening materials, the criterion based on the tensile yield stress ($\sigma_{eq} > \sigma_Y$) is applicable to define the actual plastic flow zone only at the first forward loading marking the domain where plasticity ever occurred. Because of the material's hardening it is natural to define the plastic flow zone at cyclic loading from the condition of

positive increment of the equivalent plastic strain ($d\epsilon_{eq}^{Ij} > 0$), i.e., to consider the *active*, really cyclic, plastic zone as the domain of cyclic flow and accumulation of plastic strain. Similarly to the stress-defined zones, these zones of active plastic flow are nearly independent of the load cycle number during cyclic loading at constant amplitude, and again, they look self-similar with a scaling factor of $(K_{max}/\sigma_Y)^2$. They are indeed the regions of cyclic plastic flow and accumulation of plastic strain and damage. For cyclic loading under given K_{max} , the depth of this reversed (cyclic) plastic zone at unloading ($K=K_{min}$) may be estimated as:

$$\Delta x_{PZ}(K_{max}) = 0.01 \left(\frac{K_{max}}{\sigma_Y}\right)^2$$
 (5)

where it is obvious that the cyclic plastic zone at K_{min} (unloading instant) depends on the load level represented by K_{max} . According to the numerical solutions, these active plastic zones (where $d\epsilon_{eq}^p > 0$) at load minima (reversed plastic zones at K_{min}) nearly coincide with the corresponding stress-defined domains (where $\sigma_{eq} \ge \sigma_Y$) given in Figs. 5b and 5d. At load maxima (K_{max}) the forward plastic zones shrink to 70% of their down-load counterparts, which clearly contradicts the estimation of the Rice model. In further sections of this paper the plastic zone will be stress-defined ($\sigma_{eq} \ge \sigma_Y$) for loading paths extending the plasticity domain into new regions in the material, and strain-defined or active $(d\epsilon_{eq}^p > 0)$ when the previous condition is not achieved, i.e., when further cyclic accumulation of plastic strain takes place in the previously formed plasticity domain. Thus the first definition is only applicable to the increasingly monotonic part of the first fatigue cycle and the rising loading path in the SCC tests after exceeding the maximum fatigue precracking level, i.e., for K>Kmax and this concept is associated with the forward or monotonic plastic zone whose size is given by equation (4). The second definition corresponds to the domain of cyclic plastic flow comprising the forward and reversed plastic flow zones whose sizes are assumed to be approximately the same and given by equation (5).

An original and unexpected result should be emphasized here: both the monotonic and the cyclic plastic zone sizes in the fatigue pre-cracking period (computed by nonlinear finite element analysis) are nearly independent of the load cycle number, i.e., they stabilise after a couple of cycles and remain almost constant during fatigue, in spite of the constitutive equation of the material which shows strain hardening. As a consequence, the numerical results are self-similar with the similitude criterion of $(K_{max}/\sigma_Y)^2$, in the same way as the theoretical estimations provided by Rice, although in the latter case the material is assumed to be elastic-perfectly plastic with no strain hardening at all.

Finally, it is interesting to compare the theoretical estimations of the model proposed by Rice with the results of the finite element analysis. The equations (1) and (2) of the Rice model have the same scaling factor of $(K_{max}/\sigma_Y)^2$ as the relations (4) and (5) based on the numerical computation. However, the theoretical model overestimates the monotonic and cyclic plastic zone sizes, and $x_{PZ}^{(R)}$ and $\Delta x_{PZ}^{(R)}$ are about 2.5 times the numerical values x_{PZ} and Δx_{PZ} . The Rice model predictions for the sizes of the plastic zones measured in the crack plane direction x are in better agreement with the corresponding maximum extensions r_{PZ} and Δr_{PZ} in a radial direction (see Fig. 2), following the results of the numerical analysis. The ratio $\Delta x_{PZ}^{(R)}/x_{PZ}^{(R)} = 0.25$ according to formulae (1) and (2) agrees with numerical data on average, whereas the factor 0.35 is better for the depths ratio in the crack plane direction $(\Delta x_{PZ}/x_{PZ})$ and 0.18 for the maximum extensions in radial direction $(\Delta r_{PZ}/r_{PZ})$. Equation (4) is also valid for the monotonic loading plastic zone depth $x_{PZ}(K)$ in the subsequent SCC test when $K > K_{max}$.

5. DISCUSSION

To analyze the results of the SCC tests on the basis of the performed simulation of the crack tip mechanics, it is useful to compare the characteristic distances (the plastic zone size referring to LAD, and the depth of the maximum hydrostatic stress point when HAC is considered) after

fatigue pre-cracking and during the SCC test. With regard to the latter, the critical value of the stress intensity factor for SCC to proceed, K_{QSCC} , is evaluated from the ratio of the failure load in corrosive solution F_{SCC} to the failure load in air F_{C} (Fig. 1) as follows:

$$K_{QSCC} = \frac{F_{SCC}}{F_C} K_{IC}(air)$$
 (6)

Neglecting subcritical crack growth, K_{QSCC} may be considered as an upper bound estimate for the threshold stress intensity factor K_{ISCC} , and the two characteristic values K_{QLAD} for LAD and K_{QHAC} for HAC may be considered in each particular regime. The sizes of the plastic zones at the different stages of the SCC process may be theoretically estimated by the Rice model, and numerically computed from the reported finite element results, as explained in the following paragraphs, which allows a comparison of the two approaches and an explanation of the role of fatigue pre-cracking in the stress corrosion behaviour of the steel in both cracking regimes.

5.1 Localized anodic dissolution (LAD)

Figs. 6 and 7 show the plastic zone sizes during fatigue pre-cracking (monotonic for $K=K_{max}$ and cyclic for $K=K_{min}\equiv 0$) and at the end of the LAD tests, according to the model proposed by Rice /8/ (Fig. 6) and computed by the high-resolution finite element analysis performed in this paper (Fig. 7). The similitude between the two plots is evident, and thus the Rice estimation provides a really easy first approach which reasonably predicts the trends, in spite of its not considering the strain hardening in the material. The reason for this general agreement between the two approaches may be found in the cyclic stabilisation of the monotonic and cyclic plastic zones during fatigue according to the numerical computations with a strain hardening material. However, the Rice approach clearly overestimates the plastic zones sizes, so the more detailed finite element analysis is essential to obtain a reliable and accurate picture of the evolution of the near-tip stress-strain fields.

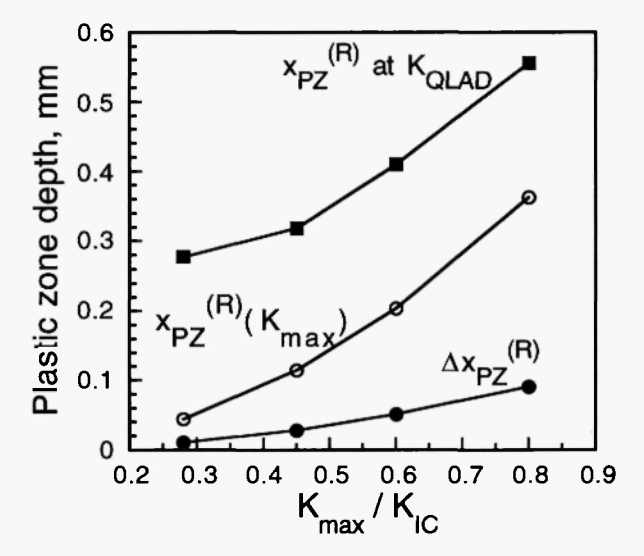


Fig. 6: Plastic zone sizes theoretically predicted according to the model proposed by Rice /8/: during fatigue pre-cracking (monotonic for $K=K_{max}$ and cyclic for $K=K_{min}$) and at the end of the LAD tests (i.e., at $K=K_{QLAD}$).

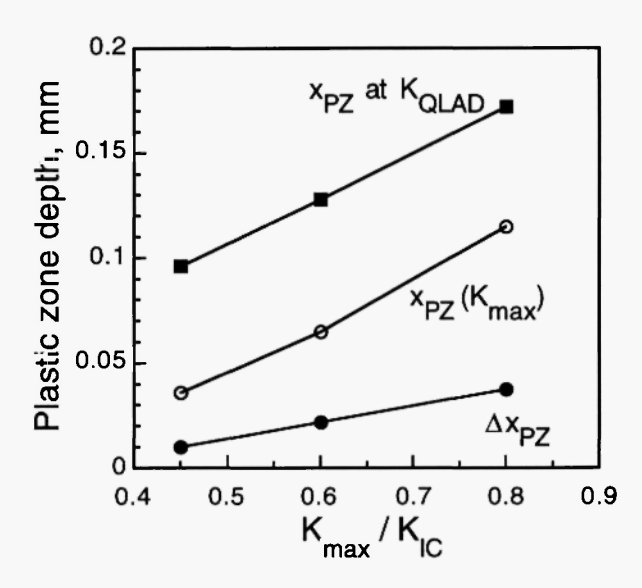


Fig. 7: Plastic zone sizes numerically computed following the procedure described in this paper: during fatigue pre-cracking (monotonic for $K=K_{max}$ and cyclic for $K=K_{min}$) and at the end of the LAD tests (i.e., at $K=K_{QLAD}$).

For LAD-controlled fracture, the fatigue pre-cracking regime causes a strong protective effect characterised by the environmentally assisted fracture load as a percentage of its

environmentally unassisted counterpart (Fig. 1), and thus the final plastic zone in the LAD test (i.e., that associated with K_{OLAD}) surpasses clearly the cyclic and the monotonic plastic zones created during fatigue pre-cracking (cf. Figs. 6 and 7). Considering the mechanical factors of pre-cracking, the normal stress variation just at the crack tip surface may be the factor capable of influencing LAD processes. In this sense, comparing the crack tip (at x = 0) stresses after pre-cracking at different ratios of K_{max}/K_{IC} (Fig. 4), their levels during SCC test were found practically insensitive to the cyclic load level K_{max} considering either the hydrostatic stress $\sigma(x=0)$ shown in Fig. 4 or a particular component σ_{yy} (x=0). Stresses in the interior at x > 0 must be irrelevant here since LAD is a surface dissolution reaction. Therefore, no difference for LAD processes should be expected from the effects of the residual stresses produced at different cycling regimes, and the crack tip plastic strains created at fatigue pre-cracking must be taken as a potentially responsible factor. The toughening effect of the fatigue pre-cracking on LAD-driven SCC may be associated with accelerated dissolution of the zone of cyclic plastic flow due to inherently higher chemical activity of the damaged (disordered) crystalline structure therein, cf. /15/, producing crack tip blunting induced by the dissolution process. Thus the increasing size of the cyclic plastic zone with the fatigue pre-cracking level K_{max} (predicted by both theoretical estimations and numerical computations, see Figs. 6 and 7) could explain the beneficial effect of fatigue pre-cracking loading on the posterior SCC behaviour: the higher the K_{max}-level, the greater the cyclic plastic zone and the more pronounced the toughening effect caused by dissolution-induced crack tip blunting.

5.2. Hydrogen assisted cracking (HAC)

Figs. 8 and 9 show the plastic zone sizes during fatigue pre-cracking (monotonic for $K=K_{max}$ and cyclic for $K=K_{min} \cong 0$) and at the end of the HAC tests, according to the model proposed by Rice /8/ (Fig. 8) and numerically computed by the high-resolution finite element

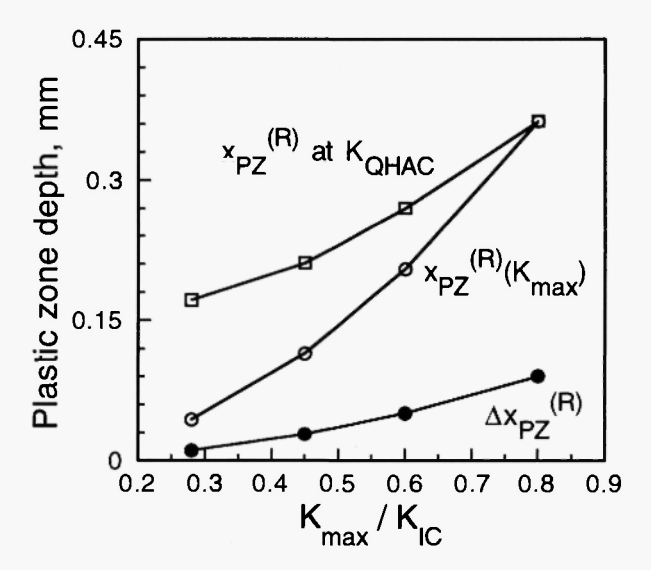


Fig. 8: Plastic zone sizes theoretically predicted according to the model proposed by Rice /8/: during fatigue pre-cracking (monotonic for $K=K_{max}$ and cyclic for $K=K_{min}$) and at the end of the HAC tests (i.e., at $K=K_{OHAC}$).

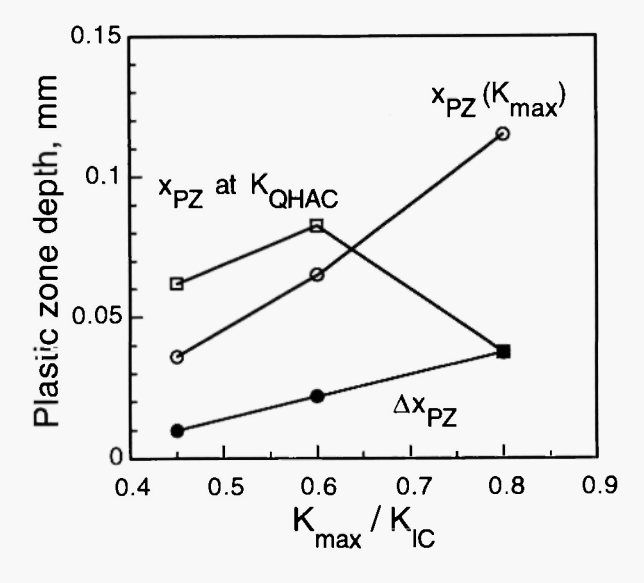


Fig. 9: Plastic zone sizes numerically computed following the procedure described in this paper: during fatigue pre-cracking (monotonic for $K=K_{max}$ and cyclic for $K=K_{min}$) and at the end of the HAC tests (i.e., at $K=K_{OHAC}$).

analysis performed in this paper (Fig. 9). As in the case of LAD, the two plots show similar trends, although the Rice approach clearly overestimates the plastic zones sizes, if compared to

the more accurate predictions given by the high-resolution numerical modelling.

It should be noted that, for lower pre-cracking K_{max} -levels, the corresponding critical values of $K_{QHAC} > K_{max}$, and the active plastic zone at fracture corresponds to the monotonic one x_{PZ} , whereas for the strongest fatigue pre-cracking regimes (higher levels of $K_{max} = 0.80$ K_{IC}) K_{QHAC} does not exceed K_{max} and the advancement of plastic straining is confined to the cyclic plastic zone Δx_{PZ} (the zone where cyclic plastic flow takes place). Just when the applied K level in a HAC test overpasses the fatigue pre-cracking level ($K > K_{max}$), the active plastic zone changes from strain- to stress-defined, i.e., from cyclic to monotonic, and this change produces a sudden increase of plastic zone size (an "explosion" of plastic zone) which is not predicted by the Rice model.

In HAC processes the global protective effect of fatigue pre-cracking loads is weaker than in the case of LAD (see Fig. 1), but the trend is the same, i.e., increasing fracture load in a hydrogen environment for rising fatigue pre-cracking level K_{max}. The explanation of this experimental fact requires a detailed modelling of the near-tip stress-strain field and not merely a simple theoretical estimation. To this end, Fig. 4 provides insight into the consequences of fatigue pre-stressing. For an intermediate level of externally applied loading in the HAC test (applied K= 0.30 K_{IC}), clear differences may be observed between the two distributions of hydrostatic stress (those associated with fatigue pre-cracking levels of K_{max} = 0.45 and 0.80 K_{IC}), especially in the close vicinity of the crack tip, which implies a different rate of hydrogen transport to prospective fracture nuclei by stress-assisted diffusion according to which hydrogen is driven by the hydrostatic stress gradient $d\sigma/dx /6/$. In the case of the strongest fatigue programme ($K_{max} = 0.80 K_{IC}$) it is seen in Fig. 4b that residual stresses remain compressive in an extended area beyond the crack tip and, what is more important, there is a negative gradient of hydrostatic stress dσ/dx<0 which delays hydrogen diffusion towards the inner points, prevents hydrogen degradation of the material therein, and increases the fracture load in a hydrogen environment.

6. CONCLUSIONS

The stress-corrosion behaviour of high-strength steel is clearly influenced by the fatigue pre-cracking procedure, since the cyclic loading regime affects the plastic zone development and controls the evolution of stress-strain fields in the close vicinity of the crack tip.

In this paper, two approaches are explored to obtain the near-tip stress-strain fields and the plastic zone development for the different fatigue pre-cracking programmes, as well as their evolution during the posterior stress-corrosion cracking tests.

The Rice model provides an easy and simple estimation of residual stress fields and plastic zone sizes after fatigue pre-cracking. However, when a more accurate and reliable calculation of near-tip stress-strain fields is required or the material has strain-hardening capacity, a high-resolution finite element analysis is required.

Both the monotonic and the cyclic plastic zone sizes in the fatigue pre-cracking period (numerically computed) stabilise after a few cycles and remain almost constant during fatigue, in spite of the constitutive equation of the material which includes strain hardening. As a consequence, the numerical computations are self-similar in the same way as the theoretical estimations provided by Rice.

Cyclic accumulation of plastic strain and creation of the domain of compressive residual stresses improve the SCC behaviour through increase of the failure load in aggressive environment either by chemical blunting of the crack tip enhanced by accumulated cyclic plastic strain (in the case of LAD) or by delaying the entry of hydrogen into the fracture process zone near the crack tip (in the case of HAC) due to the existence of negative gradients of hydrostatic stress in the vicinity of the crack tip in the most severe fatigue pre-cracking programmes.

Acknowledgements

The financial support of this work by the Spanish CICYT (Grant MAT97-0442) and Xunta de Galicia (Grants XUGA 11801B95 and XUGA 11802B97). One of the authors (VKh) is also indebted to Xunta de Galicia for supporting his stay as a visiting scientist at the University of La Coruña.

References

- 1. ISO 7539-6, Preparation and use of pre-cracked specimens (1989).
- 2. TORIBIO, J. and LANCHA, A.M. Overload retardation effects on stress corrosion behaviour of prestressing steel. *Construction and Building Materials*, **10**(7), 501-505 (1996).
- 3. NIKIFORCHIN, G.N., TSYRULNIK, A.T., TIMOFEEV, B.T., KVASNITSA, R.B. and FEDOROVA, V.A. The effect of a performed fatigue crack tip geometry on the K_{Iscc} level. *Soviet Materials Science*, **22**(6), 63-68 (1986).
- 4. HIROSE, Y. and TANAKA, K. Effect of pre-loading conditions on crack initiation and propagation in stress corrosion cracking for high strength steel. *J. Soc. Materials Sci. Japan*, **80**(29), 822-828 (1980)
- 5. ISO 7539-7, Slow strain rate testing (1989).
- 6. VAN LEEUWEN, H.-P. The kinetics of hydrogen embrittlement: a quantitative diffusion model. *Engng Fract. Mech.* **6**, 141-161 (1974)
- 7. TORIBIO, J. and LANCHA, A.M. Effect of cold drawing on susceptibility to hydrogen embrittlement of prestressing steel. *Materials and Structures*, **26**, 30-37 (1993).
- 8. RICE, J.R. Mechanics of crack tip deformation and extension by fatigue, pp. 247-309 in Fatigue Crack Propagation, ASTM STP 415, American Society for Testing and Materials, Philadelphia (1967).
- 9. KANNINEN, M.F. and POPELAR, C.H. Advanced Fracture Mechanics, Oxford University Press, New York (1985).
- 10. SURESH, S., Fatigue of Materials, Cambridge University Press (1991).
- 11. McMEEKING, R.M., Finite deformation analysis of crack tip opening in elastic-plastic materials and implications for fracture. *J. Mech. Phys. Solids*, **25**, 357-381 (1977).
- 12. TORIBIO, J. and KHARIN, V. High-resolution numerical modelling of stress-strain fields in the vicinity of a crack subjected to fatigue, pp. 1059-1064 in Fracture From Defects. Proc. 12th European Conference on Fracture (ECF-12), EMAS Publishing (1998).
- 13. HANDERHAN, K.J. and GARRISON, W.M., Jr., A study of crack tip blunting and the

influence of blunting behavior on the fracture toughness of ultra high strength steels. *Acta Met. Mater.*, **40**, 1337-1355 (1992).

- 14. MARC User Information, Marc Analysis Research Corporation, Palo Alto (1994).
- 15. FORD, F.P.Stress corrosion cracking of iron-base alloys in aqueous environments, pp. 235-274 in Treatise on Materials Science and Technology, Vol. 25: Embrittlement of Engineering Alloys, Academic Press, New York (1983).